Radio Science, Volume 20, Number 1, Pages 63–79, January–February 1985

An HF phased-array radar for studying small-scale structure in the high-latitude ionosphere

R. A. Greenwald, K. B. Baker, R. A. Hutchins, and C. Hanuise[1]

Johns Hopkins University Applied Physics Laboratory, Laurel, Maryland

(Received February 13, 1984; accepted May 29, 1984.)

Since October 1983, a new coherent backscatter radar has been in operation at Goose Bay, Labrador, for the purpose of studying small-scale electron density structure in the high-latitude ionosphere. This radar operates over a frequency band that extends from 8 to 20 MHz, and it uses an electronically phased array of 16 log-periodic antennas for both transmission and reception. The radar transmits a seven-pulse pattern that enables one to determine 17-lag complex autocorrelation functions of the backscattered signals as a function of range and azimuth. In this paper we present a complete description of the radar including explanations of the operation of the phasing matrix, the techniques of data acquisition and analysis as implemented in the radar microcomputer, and the possible on-line and automatic operating modes that may be instituted. We also present examples of some of the initial results that we have obtained with the radar during the afternoon and late evening hours. These examples include images of the two-dimensional distribution of small-scale structure and of their associated mean Doppler motion. We also present examples of *F* region Doppler spectra derived from the complex autocorrelation functions. These Doppler spectra show interesting differences from those of high-latitude *E* region irregularities.

INTRODUCTION

During the past few years there has been a significant increase in research activity directed toward phenomena occurring in the very high latitude ionosphere. While some of this increase may be attributed to the enhanced research possibilities associated with an incoherent scatter radar being located at Sondre Stromfjord, Greenland, it has also been recognized that the polar ionosphere is a region of numerous interesting, yet poorly understood, physical phenomena. One of the more interesting of these phenomena is the electron density irregularities that occur in the *F* region at high latitudes. Much remains to be learned about the mechanisms leading to their formation, the means by which they disperse over the polar cap, and the linear and nonlinear processes that lead to their ultimate dissipation (see, for example, *Kelley et al.* [1982]).

The scale size of high-latitude irregularities ranges from hundreds of kilometers down to the ion gyroradius (~ 10 m). At large and intermediate scale sizes there exists a fair body of knowledge which has been provided by incoherent scatter radar [e.g., *Vickrey et al.*, 1980; R. T. Tsunoda and J. F. Vickrey, unpublished manuscript, 1984] and scintillation measurements [e.g., *Fremouw and Lansinger*, 1981; *Livingston et al.*, 1982], respectively. In contrast, relatively little data are available at short wavelengths, even though irregularities of this scale size can be studied with ionospheric sounders. *Bates and Albee* [1970] have presented one of the early examples of small-scale irregularity research. More recently, high-latitude irregularity studies at *F* region heights have been presented by *Hanuise et al.* [1981], *Baker et al.* [1983], and *Greenwald et al.* [1983].

Several reasons exist for the sparsity of small-scale irregularity investigations in the high-latitude *F* region. Perhaps the most important of these is that the irregularity structures are magnetic field aligned. The significance of this attribute at high latitudes is shown in Figure 1. One can see that radio waves at VHF or higher frequencies undergo little refraction as they enter either the *E* or *F* regions of the ionosphere. If they encounter irregularities along their path, some of the energy in the incident wave will be scattered. However, the scattered signals obey Snell's law and are directed upward into space. In order that the scattered signals return to the radar, the incident wave must be directed normal to the irregularities in

[1]Permanently at Laboratoire de Sondages Electromagnétiques de L'Environnement Terrestre, Université de Toulon, Toulon, France.

Paper number 4S0821.
0048-6604/85/004S-0821$08.00

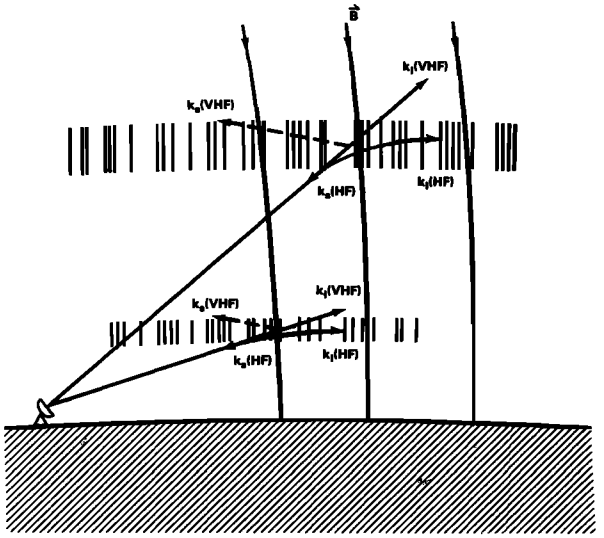

Fig. 1. Diagram illustrating manner in which VHF and UHF radar signals are scattered into space by very high latitude *E* and *F* region ionospheric irregularities. At high frequencies, the radar signals are refracted toward the horizontal as they enter the two ionospheric layers and the scattered signals may return to the radar.

the region of interest and hence normal to the magnetic field. In the high-latitude ionosphere, the normality condition can only be achieved if the ray path is refracted toward the horizontal as the wave enters the ionosphere. The refraction needed is sufficiently large that the radar must be operated at high frequencies.

Although the refraction that is required to achieve normality in any volume of ionosphere is only weakly dependent on high latitude magnetic disturbances (typically less than 1°), the high-latitude ionosphere itself is affected by both geomagnetic disturbances and diurnal variations. The associated variability in the ionospheric electron density causes an HF wave of a given frequency to undergo differing amounts of ionospheric refraction in the course of a day. At any particular time, it may be necessary to examine the ionosphere over an extended frequency band in order to determine the frequency that is best for backscatter investigations. It may also be found that more than one frequency is required to examine the entire ionospheric volume at any particular time. These considerations necessitate that the HF radar be capable of broadband operation. They also begin to indicate some of the difficulties that are associated with HF investigations.

The latitudinal and longitudinal structure of high-latitude particle precipitation also leads to difficulties in ray path determination. One way to minimize these problems is through the use of antenna arrays that are significantly more directive than those used by ionospheric sounders. Ideally, these arrays may also be steerable so that one can examine both propagation within a narrow azimuth sector and the variability of propagation with azimuth angle. Unfortunately, narrow beam, steerable antenna arrays are both difficult to construct and expensive. This is true at any frequency and especially so at high frequencies where broadband operation is desired. Consequently, equipment of this type has not been readily available for scientific investigations.

Realizing the need for improving our understanding of high-latitude *F* region irregularities and appreciating the difficulties associated with high-latitude HF investigations, we have sought to develop a unique, new radar that is particularly adaptable to this type of research. The instrument is an electronically steerable, narrow beam, phased-array HF radar operating over the 8- to 20-MHz frequency band. This instrument provides full Doppler spectral information on *E* and *F* region irregularities present in the high-latitude auroral zone, the polar cusp, and the polar cap. This paper is devoted to a description of this radar and a presentation of some of the initial results. More detailed results, including collaborative studies with other radars and satellites, will be the subject of future papers.

DESCRIPTION OF THE RADAR

The HF radar described in this paper was developed at the John Hopkins University Applied Physics Laboratory and sited at the Air Force Geophysics Laboratory field site at Goose Bay, Labrador. This is an auroral zone location at an invarient latitude of 65°. The radar transmitting and receiving array consists of 16 broadband (8–20 MHz) log periodic antennas having an array normal that is directed approximately 2° to the east of geographic north. The beam formed by this array may be directed into one of 16 possible directions ranging from 23° to the west of north to 27° to the east of north. The angular separation between beams is 3.3°. The invarient latitude interval over which useful measurements may be made extends from 2° to 20° north of the field of site.

A plan view of Eastern Canada and Greenland showing the nominal viewing area of the radar is illustrated in Figure 2. One can see that this viewing area encompasses the nominal field of view of the Sondrestrom incoherent scatter radar with which it is ideally suited for collaborative studies. The figure

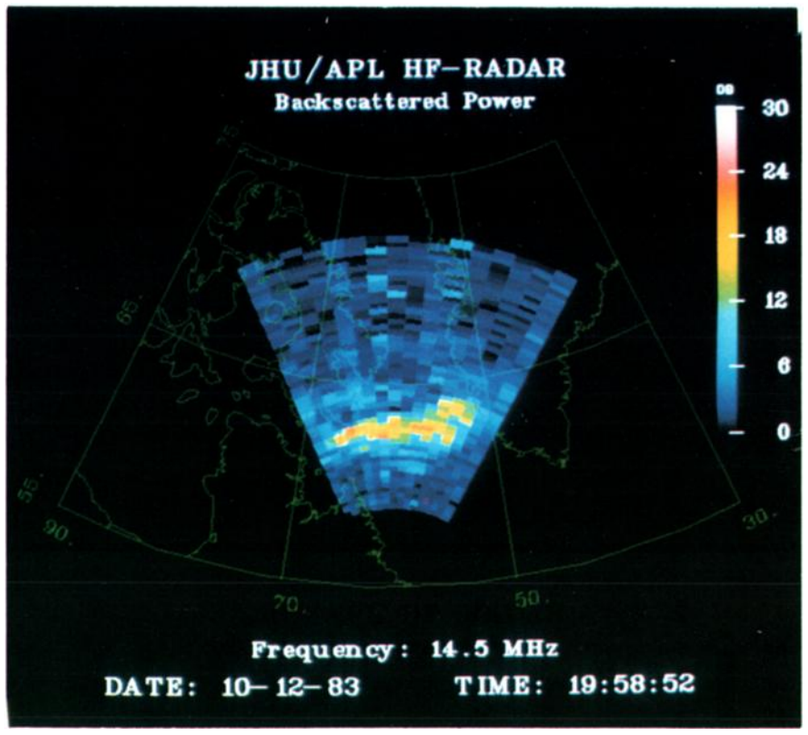

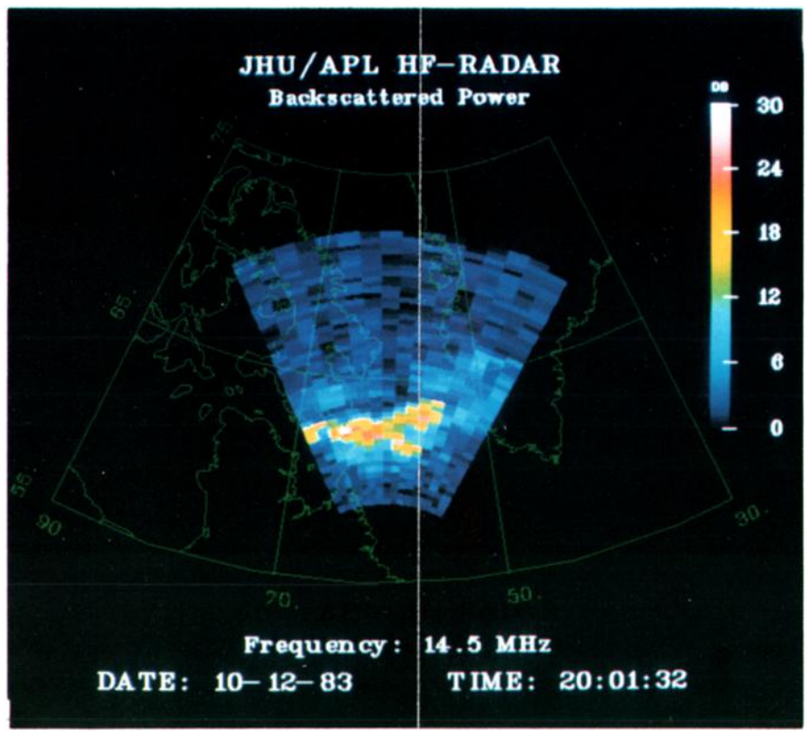

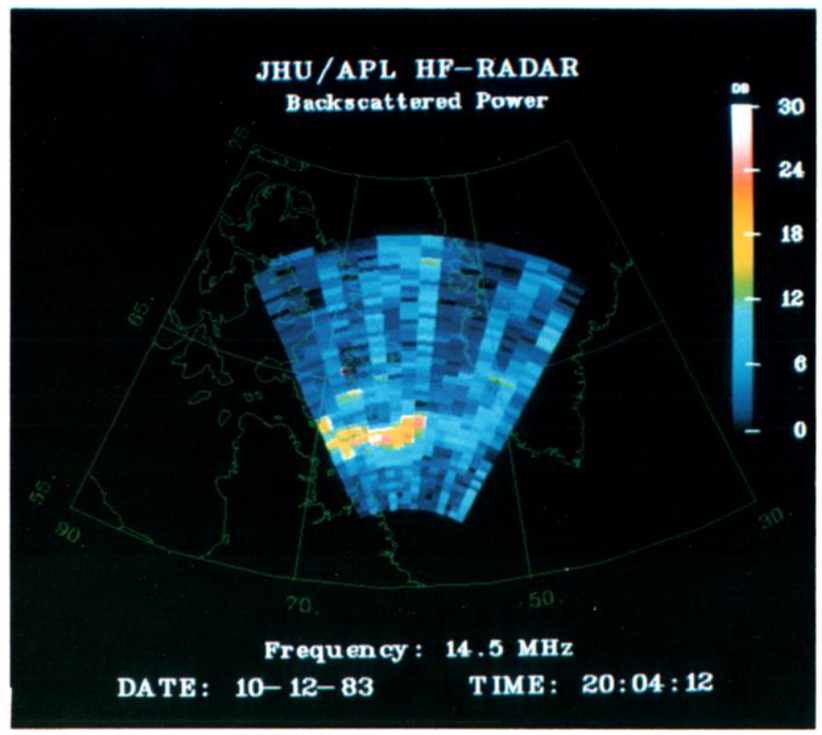

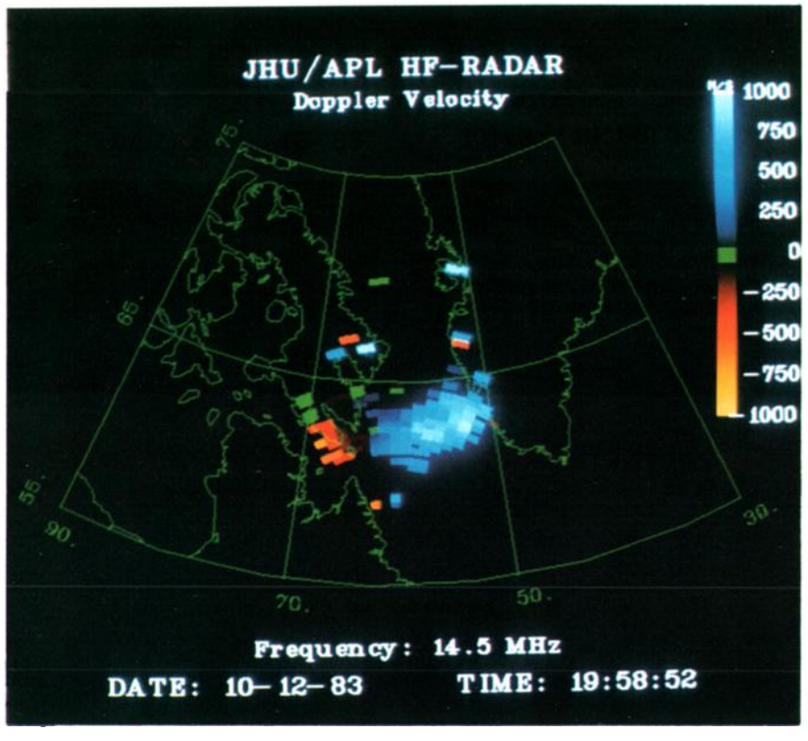

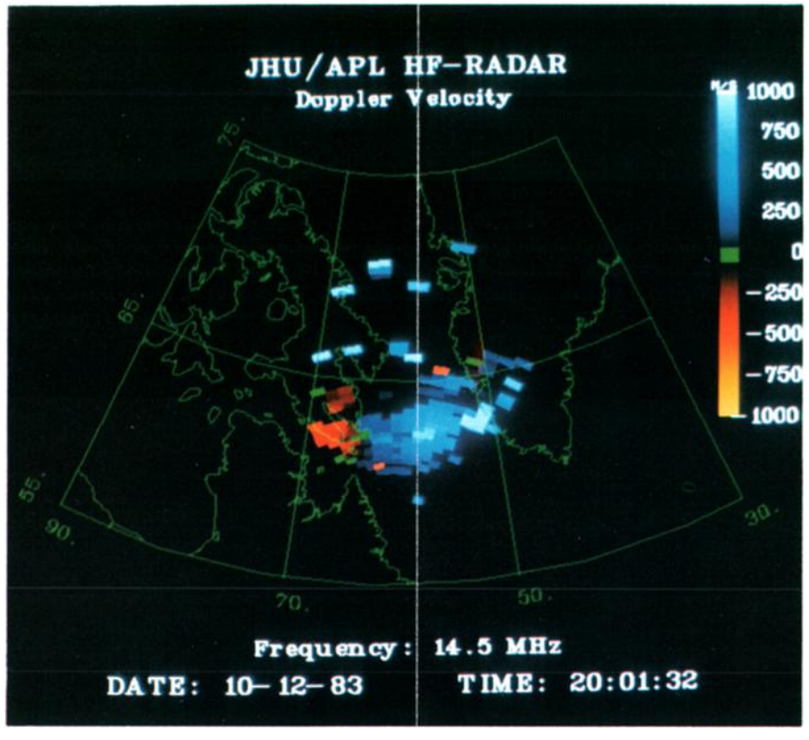

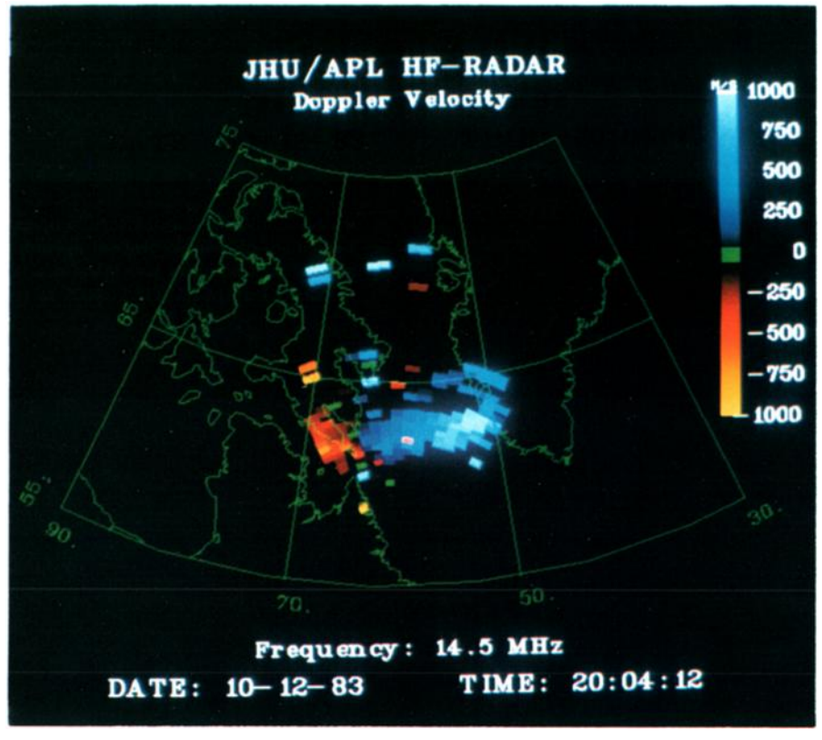

Plate 1. Sequence of backscattered power and associated mean Doppler images for October 12, 1983, 1850–2230 UT. One can see an intense region of irregularities extending between 900 and 1200 km in range and across all azimuths. Also, there is intensity structure within the scattering region that is moving from east to west through the field of view. In the highest velocity regions, the Doppler variation is consistent with drifts approaching 1750 m/s and directed toward 14° to the south of geographic west. Each image was acquired over an 80-s interval beginning at the time indicated. (*a*) Backscattered power at 1958:52 UT. (*b*) Backscattered power at 2001:32 UT. (*c*) Backscattered power at 2004:12 UT. (*d*) Mean Doppler at 1958:52 UT. (*e*) Mean Doppler at 2001:32 UT. (*f*) Mean Doppler at 2004:12 UT.

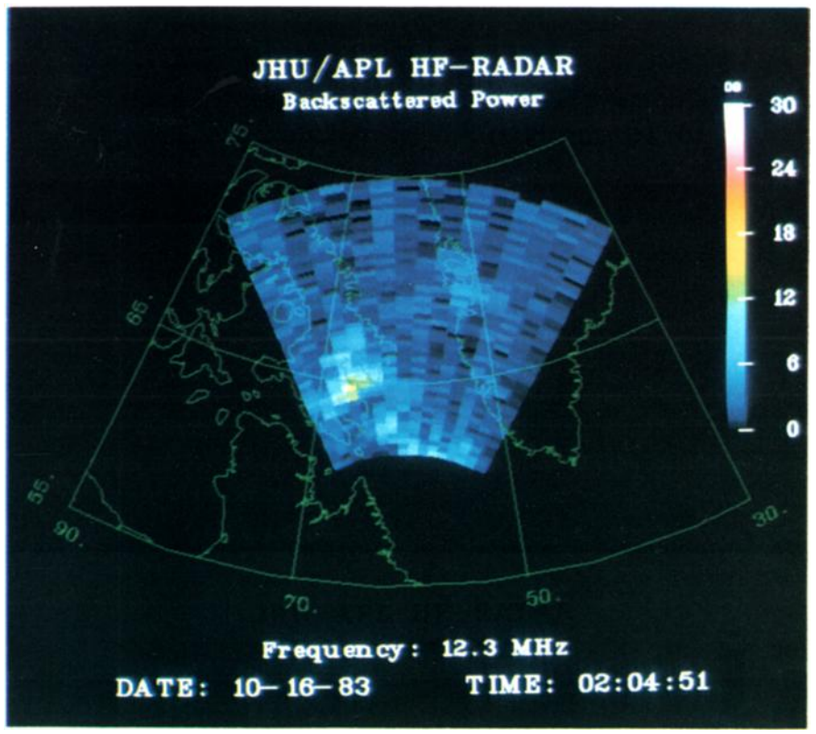

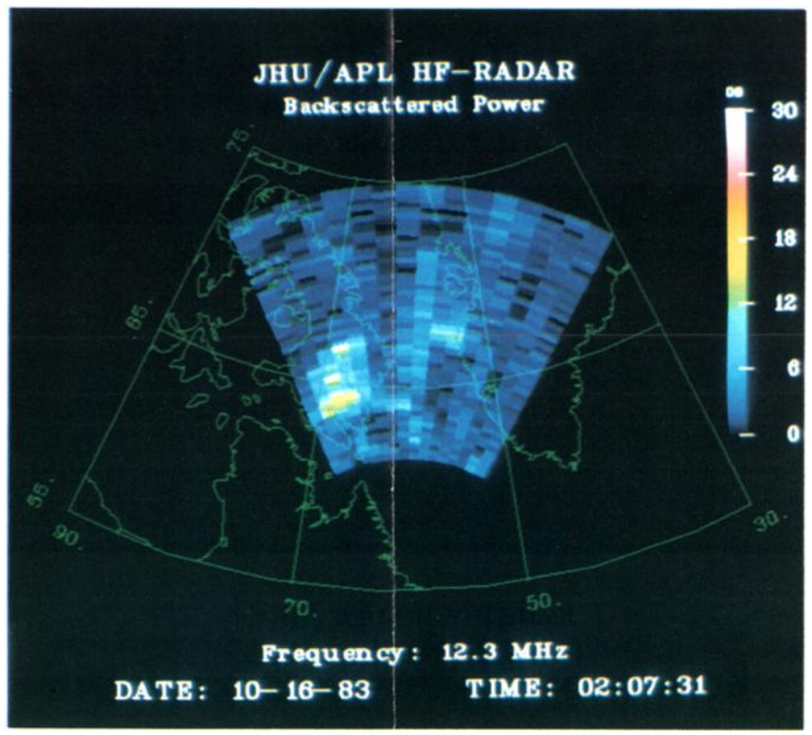

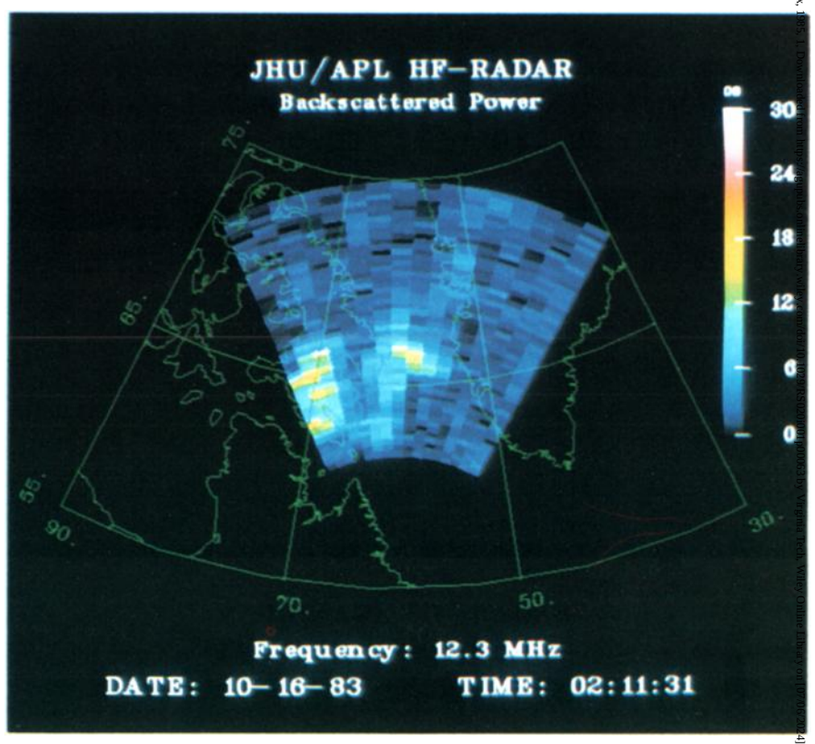

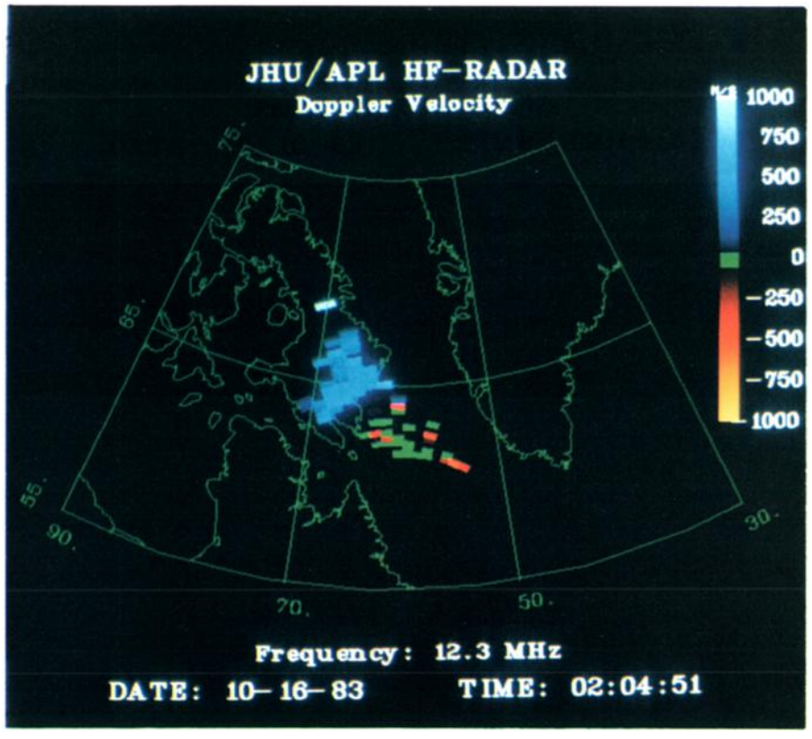

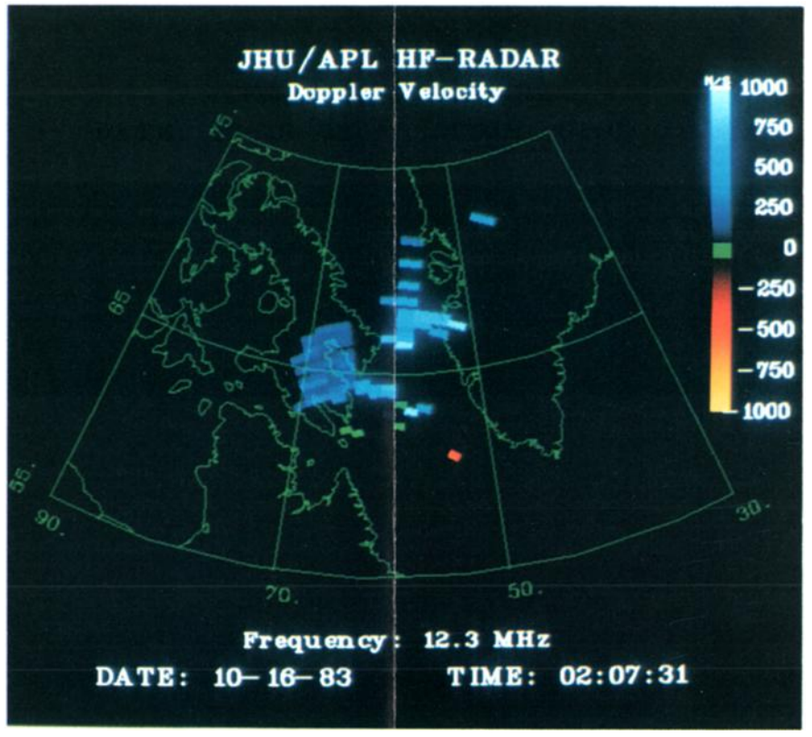

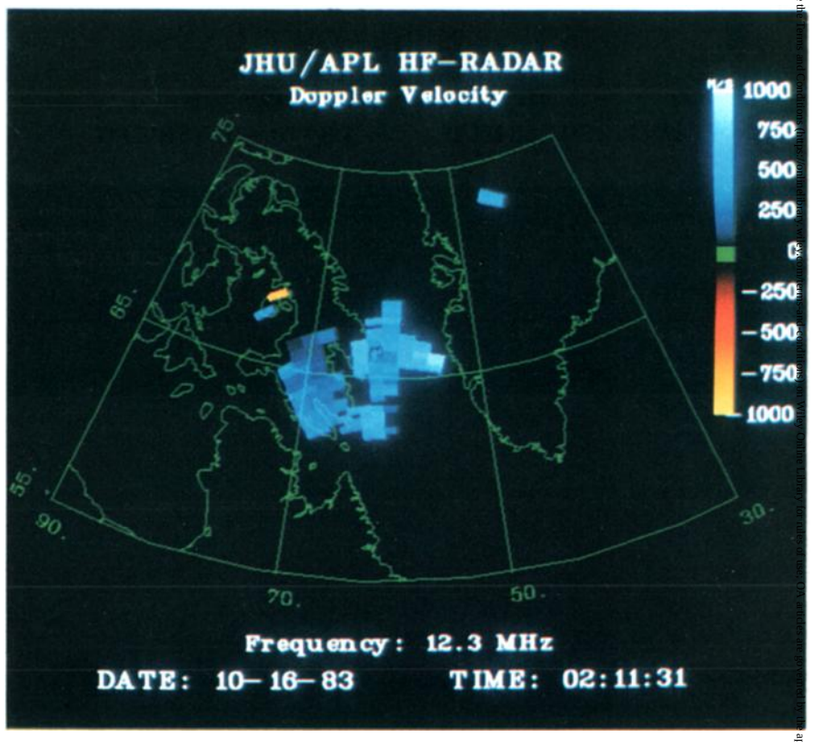

Plate 2. Sequence of backscattered power and associated mean Doppler images for October 16, 1983, 0204–0212 UT. In this example the regions of backscatter are relatively localized amorphous structures that move from northeast to southwest within the field of view. Each was acquired over an 80-s interval beginning at the time indicated. (*a*) Backscattered power at 0204:51 UT. (*b*) Backscattered power at 0207:31 UT. (*c*) Backscattered power at 0211:31 UT. (*d*) Mean Doppler at 0204:51 UT. (*e*) Mean Doppler at 0207:31 UT. (*f*) Mean Doppler at 0211:31 UT.

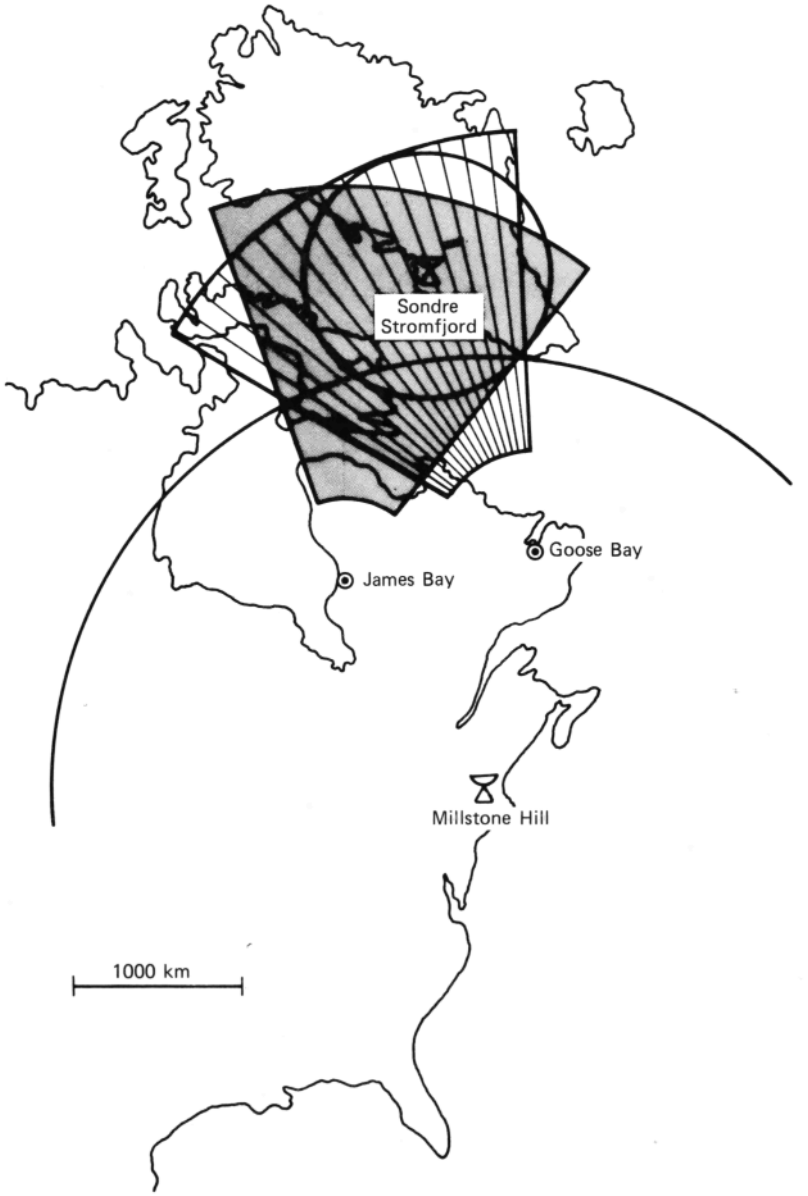

Fig. 2. Field of view of the JHU/APL HF radar located at Goose Bay, Labrador. The radar can be pointed electronically into one of 16 possible directions with a resolution cell defined by the small dark-shaded region along one of the beams. Also shown are the nominal fields of view of the Sondrestrom and Millstone incoherent scatter radars and the planned field of view (light-shaded) of a French HF radar that will be located at James Bay, Quebec. The French radar will be quite similar to the Goose Bay radar and, together, they will be used for two-component measurements of irregularity drift.

also shows the poleward portion of the viewing area of the Millstone Hill incoherent scatter radar, which also may be used for collaborative investigations. The typical spatial resolution of the Goose Bay radar is represented by the small shaded region along one of the beams in the figure. Also shown in the figure is a large shaded region, which is the field of view of a French HF radar that is presently being constructed. This radar is nearly identical to the Goose Bay facility and will be discussed more fully at the end of this paper.

Figure 3 illustrates a schematic view of the radar. The heart of the system consists of a Data General MP200 microcomputer, which controls the operation

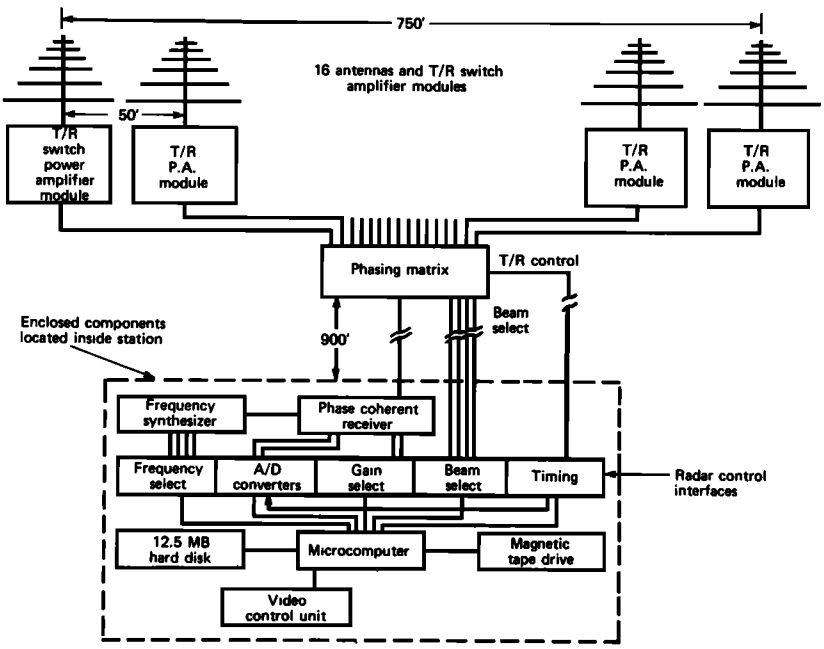

Fig. 3. Schematic view of radar. Each antenna is driven by a 75–175 W broadband transistorized power amplifier located at the base of its support tower. Each power amplifier module also contains transmit/receive switches for routing the transmitted and received power. The power supplies for the modules are located in the shed containing the phasing matrix at the center of the antenna array, and the remainder of the equipment is located in the station 900 feet from the center of the array.

of the radar as well as processes the incoming data. Two modes of operation are possible. In one, radar operation is controlled by an on-site operator through parameters entered from the display terminal. This mode is used for campaigns at the field site and may be thought of as the interactive mode. The other mode is used for noninteractive operation. It utilizes a schedule of predefined operating times and frequencies. In the latter mode, command strings read from a disk file, direct the radar through a series of operations. The disk files may be prepared days or weeks in advance.

After the relevant radar operating parameters are entered by either an operator or the predefined schedule, radar operation is controlled by the digital input-output interface (DIO) and the timing sequencer. The DIO is used for non–time-critical operations such as changes in the operating frequency or control of the receiver gain. Time critical operations are controlled by the timing sequencer. This interface utilizes a direct memory access channel and receives control words from the computer memory. The words, as shown in Figure 4, determine the time to the next control word transfer, the status of the calibration pulse, the status of the transmit/receive (T/R) switch, the status of the RF pulse, the status of the sample

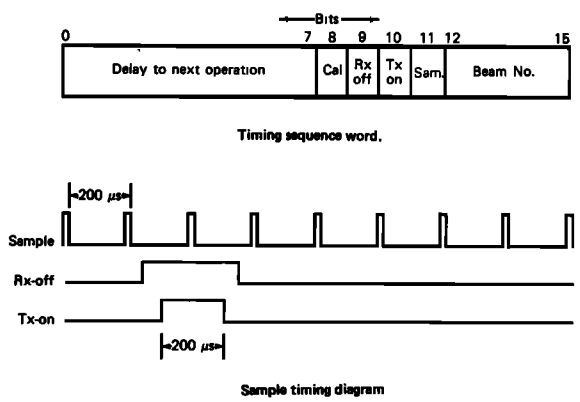

Fig. 4. Examples of timing sequencer control word and timing sequence. All time-critical radar functions are under the control of the timing sequencer. This device is a direct memory access-controlled buffer that receives 16-bit words from a software-generated timing sequence array within the computer memory. The bits of these control words determine the time delay to the next control word transfer, the status of the calibration signal at the input to the receiver, the status of the transmit/receive switch, the status of the transmit pulse, the status of the sample gate, and the antenna beam selected. Generally, the timing sequence is less than 500 words in length.

gate, and the number of the selected antenna lobe. Although the minimum possible transfer separation is 10 μs, the typical time between control word transfers is 100–200 μs. The control words are defined by a software subroutine which derives them from the radar operating parameters. In most cases the length of the control word sequence is around 500 words.

The transmitted RF signal is generated within the receiver unit and amplified to a signal level of 2W. This signal is directed to the phasing matrix which is located at the center of the antenna array. There, it is divided into 16 component parts. Each of these component signals are given a relative time delay that is appropriate for the selected beam direction.

A schematic view of the phasing matrix is shown in Figure 5. The principal elements of the matrix are the eight phasing networks which we will refer to as "phasing trees." On transmission, signals enter a "tree" from the receiver side and pass through a branching network of power dividers and lengths of cable that ultimately produce a relative time delay between successive outputs. On reception, signals enter the "tree" from the antenna side and are reformed into a composite signal. Those signals arriving from the direction into which the antenna array is directed will undergo constructive interference and exit the array at a considerably increased power level. It is important to note that the use of delay lines in the phasing matrix leads to constant time

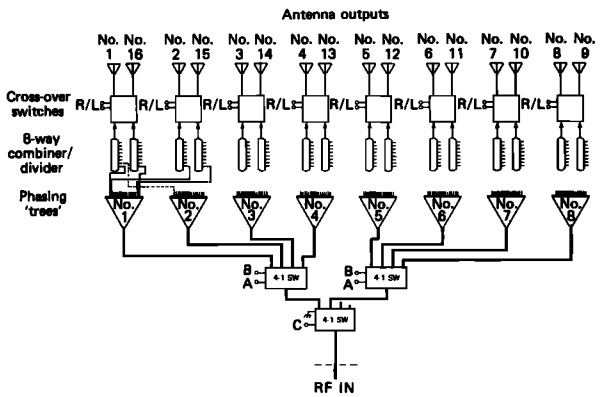

Fig. 5. Schematic view of phasing matrix. This device establishes a progressive time delay across the antenna array on transmission and reforms the beam on reception. The 4-1 switches select one of eight possible branching networks (phasing "trees"). Each "tree" consists of power dividers and delay lines that produce a specific time delay across the 16 outputs and represent one possible beam direction. The crossover switches determine whether the selected beam points to the right or left of the array normal. On reception, the process is reversed and the matrix reinforces only those signals from the preselected direction.

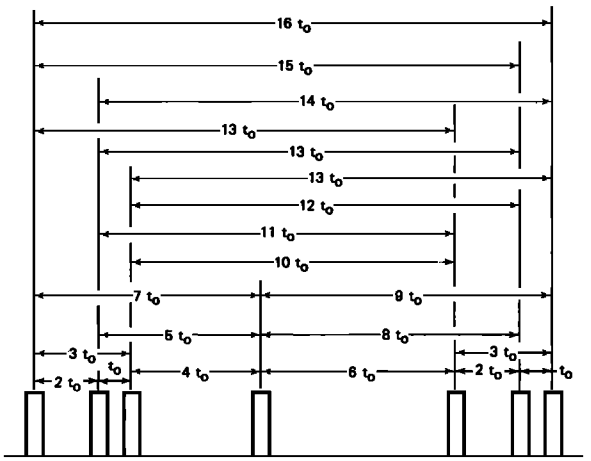

Fig. 6. Seven-pulse sequence used to determine 17-lag autocorrelation functions of the backscattered signals. Typically, $t_0 = 3$ ms. This sequence has range redundancy for lags t_0, $2t_0$, $3t_0$, and $13t_0$. The first three lags do not introduce ambiguity due to the large group delay time ($10t_0 = 30$ ms) between their repetition. The last lag has range ambiguity, but generally does not have a significant influence on the resulting Doppler spectra.

delays and not constant phase delays. The former are required to obtain frequency-independent steering of the beam.

Each "phasing tree" produces one possible set of time lags across the antenna array. The four-way switches in Figure 5 are used to select one of the "phasing trees," while the double-pole, double-throw switches (crossover switches) determine whether the selected beam is to the right or left of the array normal. The properly phased RF signals at the output of the phasing matrix are then directed to the T/R switch, amplifier modules at the base of each antenna. On transmission the switches are gated so that the signals pass through the amplifier chain and achieve a pulsed power level that varies from 75 W at 20 MHz to 175 W st 8 MHz. The variation in output power is due to both the 23-MHz low pass filter at the output of each amplifier and the increased cable losses at the higher frequencies. While these power levels do not seem high, one must appreciate that much is gained from the large number of amplifiers and from the array factors. The average peak radiated power from the array is 2 kW, and the effective radiated power is nearly 200 kW.

On reception, the T/R switches are gated so that the return signals pass directly through the modules and to the phasing matrix. There, the signals from the direction of the selected beam are reinforced and passed on to the receiver. The receiver is phase co-

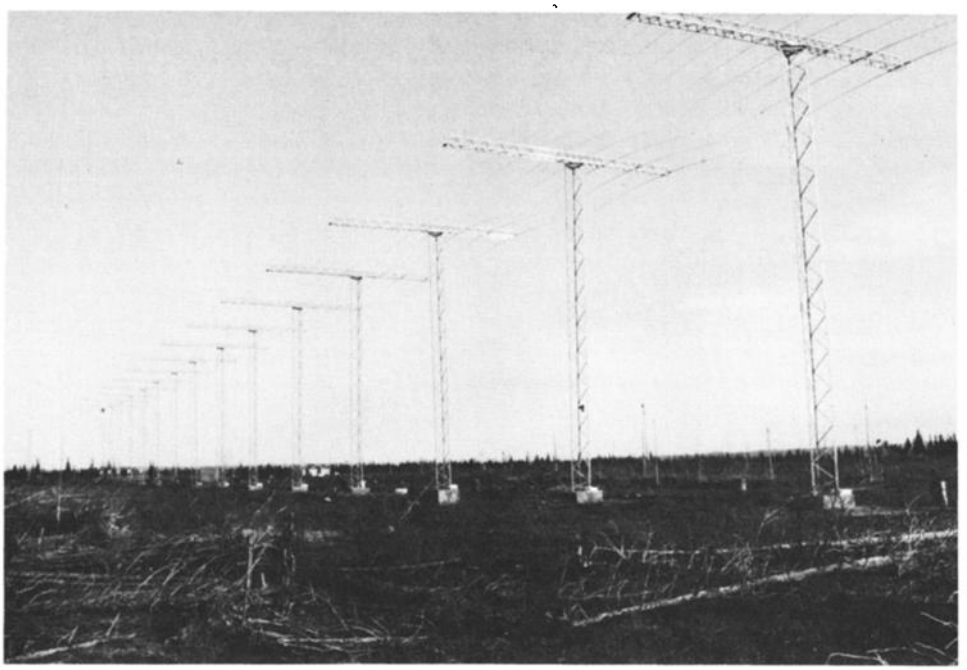

Fig. 7. View of antenna array from front, northwest corner. Shed for phasing matrix is located at the center of the array.

herent with baseband quadrature outputs. These are sampled by the microcomputer and processed in a manner that is consistent with the transmitted pulse pattern.

In most instances the radar transmits a multipulse pattern that has been described by *Greenwald et al.* [1983]. For completeness, this pattern is shown in Figure 6. The on-line microcomputer samples the received signals resulting from this transmitted pattern and calculates, in real time, 17-lag complex autocorrelation functions for a number of distinct ranges. These autocorrelation functions are subsequently transformed into 32-point Doppler spectra at the Applied Physics Laboratory.

Multipulse investigations are extremely useful if one must resolve the ambiguity that occurs when the Doppler shift or bandwidth of the backscattered signal requires an interpulse period (IPP) that is less than the group delay extent of the scattering region. In the case of high-latitude investigations at HF frequencies, Doppler bandwidths and/or shifts in excess of 100 Hz are relatively common. To resolve these, a sampling frequency of 200 Hz and an IPP of 5 ms would be required. Unfortunately, high-latitude backscatter often extends over appreciably more than 5 ms in group delay and the range to the scattering volume becomes ambiguous. The multipulse mode eliminates this ambiguity by reducing to one the number of ranges that can contribute to most lags of the autocorrelation function.

Farley [1972] has considered a number of multipulse patterns that might be used for radar autocorrelation function studies. Unfortunately, many of these patterns do not contain all of the lags of the autocorrelation function. We have developed the alternative pattern, shown in Figure 6, which contains all of the lags of the autocorrelation function. While this pattern has range ambiguity for lags t_0, $2t_0$, $3t_0$, and $13t_0$, the potential problem at lags t_0, $2t_0$, and $3t_0$ is eliminated by the large time lag ($10t_0$ or typically 30 ms) between the repetition of these lags. The ambiguity at $13t_0$ is argued away by the relatively weak correlation that exists at a lag of $13t_0$. Consequently, even if several distinct ranges contribute to this lag of the autocorrelaton function, they should not affect the resulting Doppler spectra to any great extent.

As noted previously, the transmitting and receiving array used in the Goose Bay HF radar consists of 16 log periodic antennas. A photograph showing 15 of these antennas is seen in Figure 7. (The remaining antenna crashed into the ground during the construction phase. It is presently being repaired and will be reerected in the summer of 1984.) Each an-

tenna has a half power beamwidth of 60° or better over most of its operating band. The array has an overall length of nearly 240 m, stands at a height of 15 m, and each antenna is approximately 12 m in length. The two-way half power width of each of the beams formed by the array varies from 2.5° at 20 MHz to 6° at 8 MHz.

Figure 8 exhibits the theoretical two-way azimuthal patterns of the eight beams to the right of the array normal. An identical set of eight beams exists to the left of the array normal. Their patterns are the mirror image of those presented here. Below 16 MHz there are no grating sidelobes of any significance, and other sidelobes are down by more than 27 dB. Above 16 MHz grating sidelobes begin to appear for the outermost beams. That is, at 18 MHz beam 8 to the right of the array normal has a grating sidelobe at −44°, beam 7 has a grating sidelobe at −48°, etc. To reduce the undesirable effects of these sidelobes, one might choose not to use the outermost beams at the higher frequencies. While this is a potential solution, we have as yet not observed any ambiguities due to their presence.

The vertical pattern of the antenna array is quite broad with an average half power beamwidth of ~30°. At 8 MHz, this beam maximizes at an elevation angle of approximately 35°, whereas at 20 MHz, the maximum occurs at an elevation angle of 15°.

As previously noted, the backscattered signals from the multiple transmitted pulses are sampled by the microcomputer. Typically, samples are obtained for 50 discrete ranges with a sample separation of 15–30 km. The autocorrelation functions of the backscattered signals for each range are then calculated using the lag separations derived from Figure 6. Concurrently, the next multipulse transmission pattern is transmitted and the backscattered signals from these pulses are sampled. The analysis procedure described here effectively limits the multipulse pattern repetition time to the greater of (1) the multipulse pattern length with a suitable delay before the pattern is repeated or (2) the calculation time of the 50 autocorrelation functions. In our case the former time is 70–80 ms, whereas the latter is ~100 ms. Thus we have an effective pattern repetition frequency of ~10 s^{-1}.

Range-dependent autocorrelation functions of the backscattered signals are accumulated for some preselected integration interval (typically 5–10 s). At the end of this period the accumulated data along with the radar operating parameters are written onto magnetic tape and some reduced form of the data is

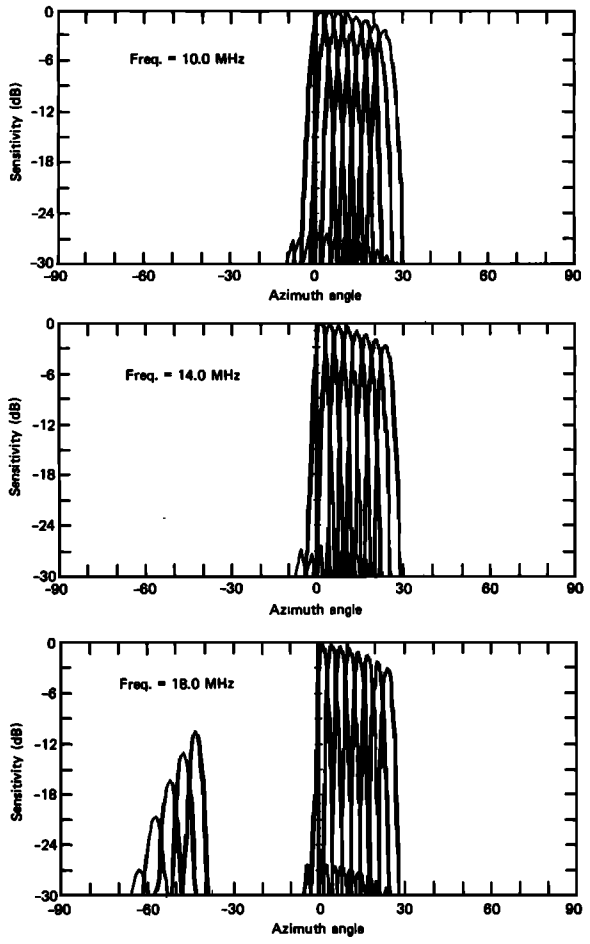

Fig. 8. Theoretical two-way azimuthal patterns for eight lobes to the right of the array normal at frequencies of 10, 14, and 18 MHz. Lobes at negative angles for 18 MHz case represent grating sidelobes of rightmost lobes. An additional mirror image set of patterns exist to the left of the array normal.

plotted on the console display unit. At the present time, three display presentations have been developed. These are (1) backscattered power as a function of range and beam, (2) Doppler velocity as a function of range and beam, and (3) selected autocorrelation function.

Figure 9 exhibits an example of a real time backscattered power plot. In this figure the 50 ranges extend from left to right, and the 16 beams (numbered 0–15) extend downward. Beam 0 is the most counterclockwise beam, and the numbering increases upward in a clockwise fashion. Times in this and in subsequent figures are given in universal time, the frequency is 9.31 MHz, and the beam number represents the beam that was used during the preceding

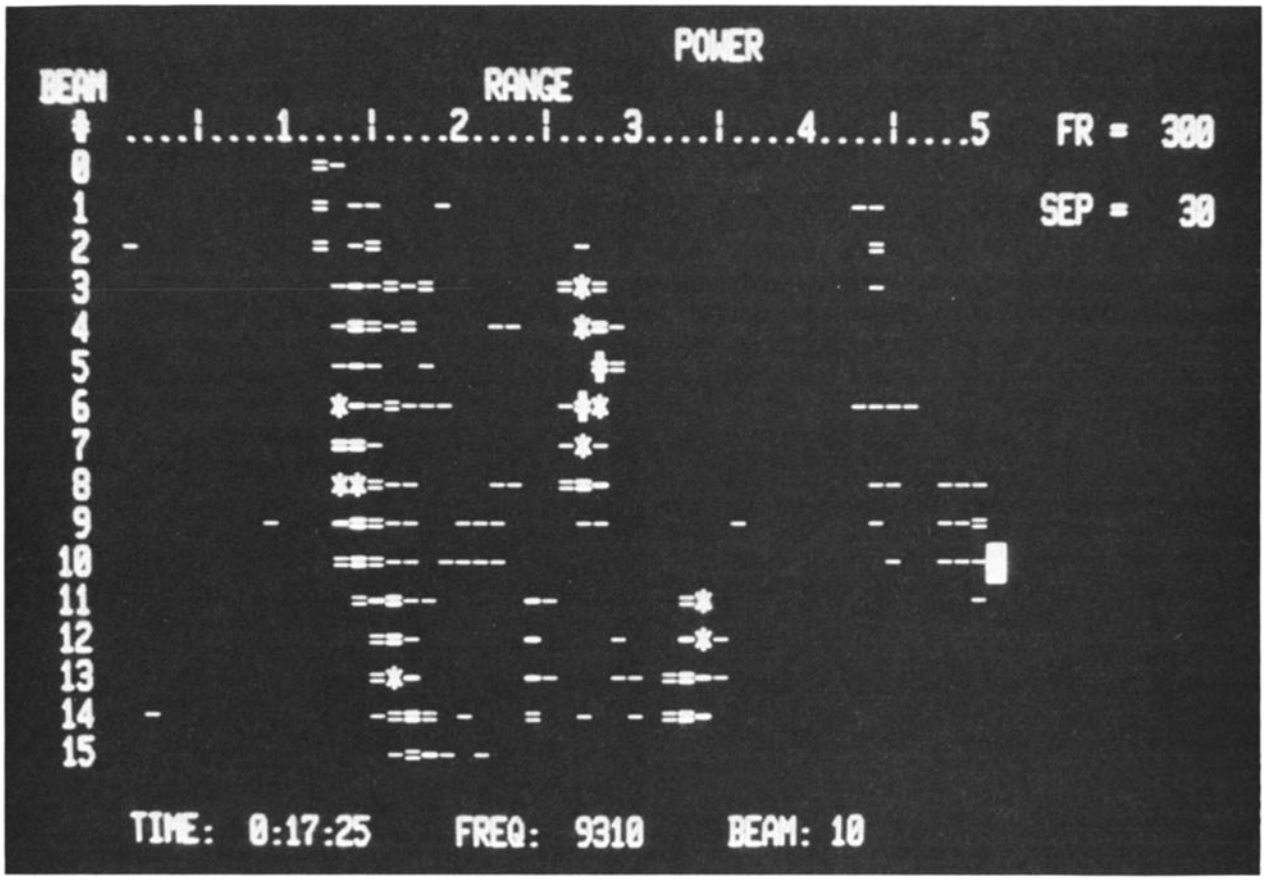

Fig. 9. Sample plot of backscattered power versus beam and range from station on-line display. Range increases to the right, and beam number is plotted vertically with the most counterclockwise beam at the top and the most clockwise at the bottom. The signal levels are gray scale coded in steps of 3 dB. FR is the first range, in this case 300 km, and SEP is the separation between range samples (30 km). The most recently plotted viewing direction was beam 10 for which the frequency of operation was 9.31 MHz. (Photograph courtesy of John Kelsey, Canada Marconi).

integration period. The label FR defines the range in kilometers to the first range gate, and the label SEP defines the separation between range gates, again in kilometers. The characters on the display provide a crude gray scale code of the location and intensity of the backscattered signals.

The backscattered power plots provide a two-dimensional representation of the intensity of regions of irregularity and/or ground backscatter as a function of range and azimuth. The image is continuously updated, with the power profile for each beam being plotted at the completion of its integration interval. If the radar is operating in a 5-s integration mode, then the entire image is updated every 80 s. In general, it is possible to use this display mode to observe the bulk motion of extended regions of irregularity backscatter.

The Doppler velocity plots are similar to the backscattered power plots in format. However, the gray scale code is replaced by integers in direct and inverse video which define the magnitude and sense of the line-of-sight Doppler velocity.

The third display format is the autocorrelation plot shown in Figure 10. In this mode one may select the range for which the autocorrelation function will be plotted, or allow the computer to select the range with the largest backscattered power. This example illustrates the autocorrelation function for range 8, which has a signal-to-noise ratio in the range 6–9 dB. One sees that the autocorrelation function is quite well behaved, a feature that is characteristic of most of our data. Also, the decay of the autocorrelation function is relatively slow, indicating that the associated Doppler spectrum is relatively narrow. This

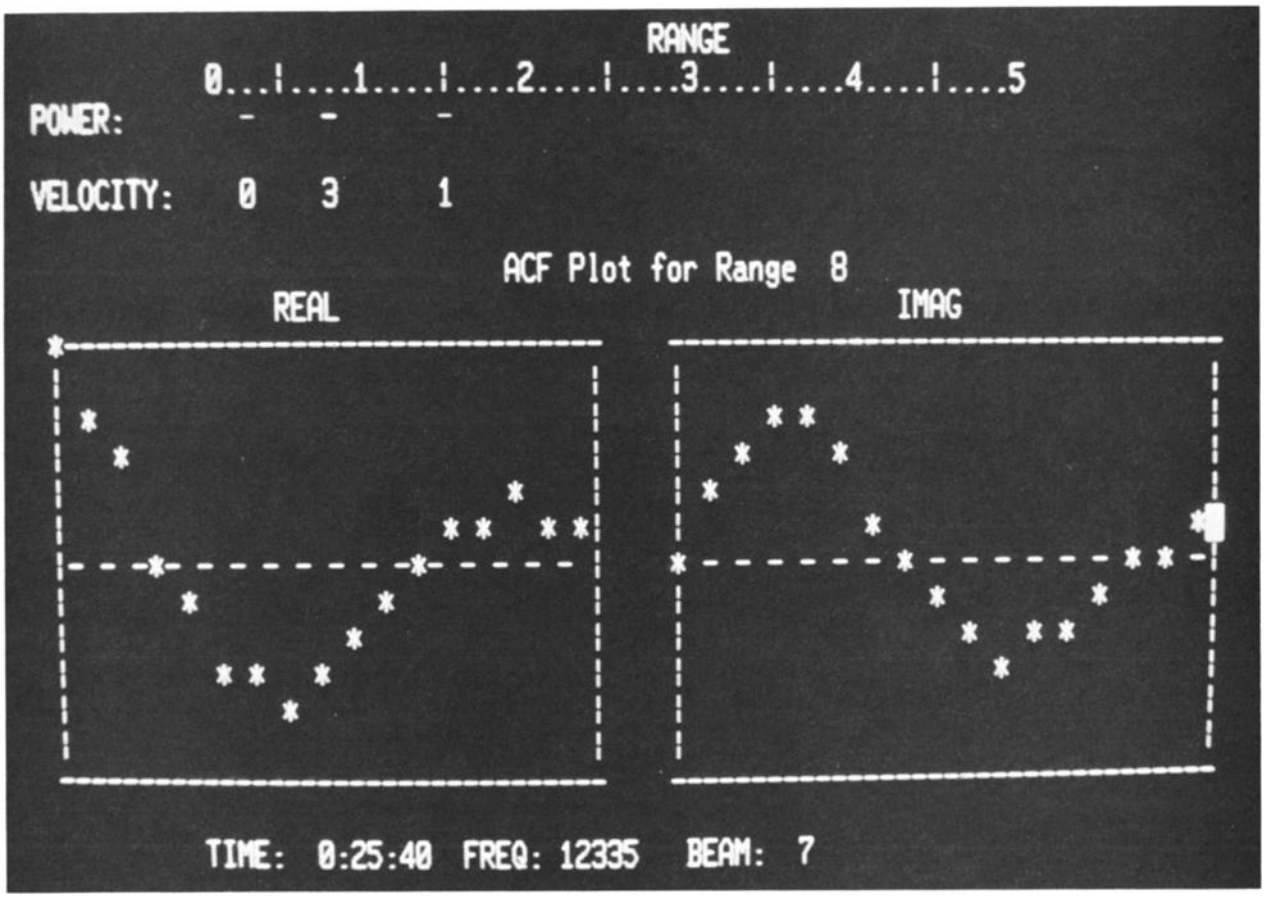

Fig. 10. Example of an autocorrelation function of the backscattered signal as plotted on the station on-line display. The ACF may be plotted for a selected range or for the range with the largest backscattered signal level. Also plotted in the figure are the backscattered power and Doppler profiles of the previous integration. In this example, the snr of the signal plotted was in the range 6–9 dB. (Photography courtesy of John Kelsey, Canada Marconi).

point will be discussed in more detail later in this paper and in subsequent publications.

Note also, that the autocorrelation plots show the power and Doppler velocity profiles of the previous integration interval and beam direction.

OPERATION OF THE RADAR

Having highlighted many facets of the Goose Bay radar, we now present a comprehensive view of the radar in operation. By way of illustration we will consider the sequence of operations that occur when the radar is running in the beam priority mode. This mode scans the radar beam at each operating frequency. A flow diagram of the mode is shown in Figure 11. One can see that for this mode, as for others, operation is initiated by commands entered from the console keyboard or a command file. These commands include definitions of the frequency table and the beam table. The frequency table consists of up to 16 preselected 100-KHz frequency bands within the 8- to 20-MHz frequency interval that might be studied at any particular time; the beam table consists of up to 16 beam numbers. Neither the beam numbers nor the frequencies need to be in any particular order, nor do they need to be nonrepetitive.

In most instances the analysis is initiated with an ionospheric sounding. This is a subroutine in which the radar is scanned over the frequency table to determine those frequencies for which ionospheric backscatter is observed. From these, a predefined number are selected for more detailed analysis. The radar then begins with the first selected frequency and proceeds to step through the beam table. For each beam, the radar is first scanned through the

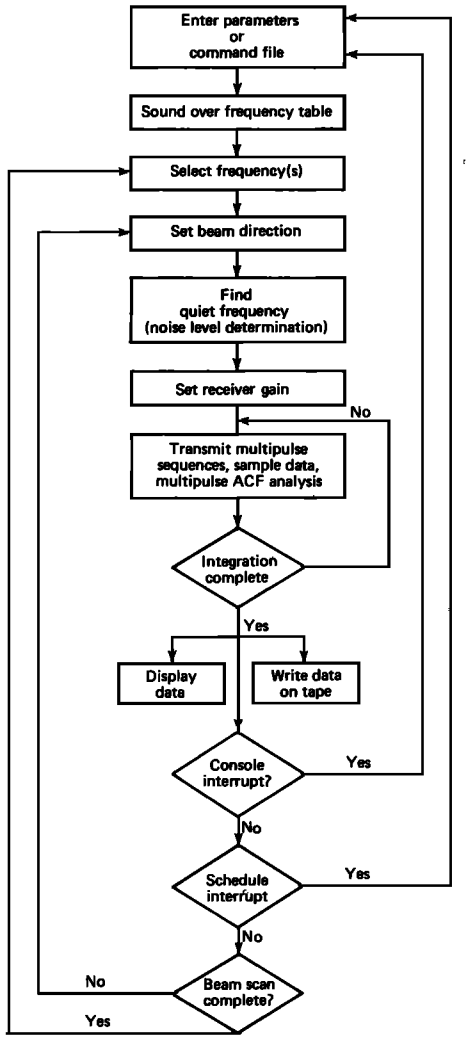

Fig. 11. Flow diagram of HF radar operation under beam priority. In this mode the radar scans through a table of beam directions while operating in a particular 100-kHz-wide frequency band. It then proceeds to the next frequency band and repeats the beam scan. It is also possible to have frequency priority operation in which the radar scans through a table of frequencies for each beam direction.

100-KHz frequency band to determine the least disturbed 5-kHz-wide region within it along with the noise level for that region. It then transmits on that frequency and the receiver gain is adjusted so as not to overload the receiver with strong returns. Next, the radar proceeds with the multipulse analysis for the specified integration time. Upon completion, the data are written on tape and the selected display format is plotted on the video console. Checks are then performed to determine if interrupts had been generated from the console or from the schedule. If not, the beam is switched to the next entry in the beam table, or, if the beam scan is complete, the entire scan is repeated at the next selected frequency. A console interrupt will allow new parameters to be entered and the program restarted. A schedule interrupt may cause the entire program to be paused or restarted, or it may reinitiate operation of the Sounder subroutine and produce new selected frequencies.

INITIAL RESULTS

Since October 11, 1983, when the JHU/APL radar at Goose Bay was put into operation, it has operated on a near daily basis. In this paper we present two examples of some of the initial data obtained with the radar. These examples demonstrate the capabilities of the radar and illustrate the character of very high latitude *F* region irregularities as they appear in the afternoon and late evening local time sectors.

On October 12, 1983, ionospheric backscatter was observed continuously from 1850 to 2230 UT (1450–1830 LT). It was first observed over the range interval extending from 1400 to 1800 km; however, with time it migrated equatorward and then poleward. The period considered here covers the time interval 1958–2004 UT when the scattering region extended from 900 to 1200 km in range. At these ranges the source of the scattered signal might be located in either the *E* region or the *F* region of the ionosphere; however, there are several reasons why we believe that the scattering volume is located in the *F* region. First, the scattering region was first observed at ranges for which the *E* region would be well under the horizon. Second, an *E* region source at ranges of 900–1200 km would require that the signals were returning from elevation angles of less than 3°. At these low elevation angles the antenna array has relatively poor sensitivity. Finally, the character of the observed Doppler spectra is quite different from the spectral character of *E* region diffuse radar aurora observed in the same local time sector. (We will discuss this point more fully later in the paper.)

During the period of interest the radar was operated in a 16 beam scan mode with a dwell time of 5 s per beam. Thus every 80 s it was possible to obtain an image of the backscattered signal level as a function of range and azimuth. By assuming the irregularities to be located at a particular height—we have assumed 300 km—it is possible to project the regions of backscatter onto a geographic grid. If the actual height of the irregularity layer were higher/lower than the assumed height, then the projected location

of the irregularities would be equatorward/poleward of the location shown.

Three images of this two-dimensional projection for the time interval 1958–2004 UT are shown in Plates 1*a*–1*c*. Also indicated in the plates are outlines of the North American and Greenland land masses. One sees that the irregularities are observed over a large region and that they are significantly more extended in longitude than in latitude. Moreover, there is clearly observable longitudinal structure which is drifting in a generally westward direction. We have chosen to plot every second image in order to emphasize this drift. (It should be noted that the increased background noise along some of the beams of Plate 1*c* is due to disturbance transmitters being received by the radar.)

In order for large-scale structure to remain identifiable as it drifts through the radar field of view, it is necessary that (1) the irregularity cross section be approximately independent of the angle between the radar wave vector and the irregularity drift direction, (2) the conditions leading to the formation of small-scale irregularities remain approximately constant during the period of observation, and (3) the propagation conditions remain approximately constant. While we do not have any specific knowledge that these conditions hold, our ability to track this structure through the field of view seems to indicate that it is so. Since our initial data set has yielded many other examples of ionospheric structure moving through the field of view without losing its identity, it appears that this phenomenon is not too uncommon.

From the westward displacement of the structure and the time of observation, one can estimate the westward drift velocity. For the example shown, the average velocity of the entire structure is approximately 1000 m/s. This velocity is typical of the convective drift velocities that are observed in the high-latitude ionosphere in the afternoon sector.

Plates 1*d*–1*f* show the mean Doppler velocity images associated with Plates 1*a*–1*c*. These Doppler determinations have been obtained by using all significant lags of the autocorrelation function for any beam and range. Values have only been determined if the strength of the backscattered signal is greater than the receiver noise level. In general, only the extended region of Doppler data, i.e., the extended region of blues and reds near the center of each plate, is meaningful data. The remaining isolated Doppler values are most likely noise that has passed through our Doppler discriminator.

Several interesting features may be seen in the Doppler data. First, one notes that there is a dark region between the red and blue Doppler values. This region is not due to an absence of backscattered signals but to the presence of very low Doppler values ($|V_p| < \sim 50$ m/s). These low values lie along the mean direction of beams 3 and 4 in Plate 1*d* and along beam 3 in Plates 1*e* and 1*f*. The pointing direction of these beams ranges from 13° to 16° to the west of geographic north. One can conclude that the drift of the irregularities is approximately normal to this direction. Furthermore, by noting that the Doppler values become increasingly positive as the radar is directed more toward the east and increasingly negative as the radar is directed more to the west, one can conclude that the irregularities are drifting in the direction of 13°–16° to the south of geographic west. This mean drift direction showed little variation over the 7-min interval of these observations.

Closer examination of Plates 1*d*–1*f* reveals some interesting fine structure within the Doppler maps. One sees in Plate 1*d* that there are two localized regions within the approaching Doppler field where the Doppler velocity reaches 1000 m/s. These are centered on beams 10 and 13. In Plate 1*e* there are three enhanced Doppler regions centered on beams 6, 9, and 14 or 15. One can assume that in the 160-s period between the two Doppler maps, the enhanced Doppler regions on beams 10 and 13 of Plate 1*d* had drifted into beams 6 and 9 of Plate 1*e*. The enhanced velocity region on beams 13–15 indicates that an additional enhanced Doppler region is entering the field of view from the east. Under this scenario the relatively low value of the enhanced Doppler region on beam 6 of Plate 1*e* may be explained by the fact that the region has moved so that the drift is nearly perpendicular to the radar line of sight. Also, one can use the westward displacement of the original two regions of enhanced Doppler to estimate their westward drift velocity. In both cases, the enhanced velocity regions traversed approximately 260 km in the 160-s period, indicating a westward drift of approximately 1600 m/s.

Plate 1*f* lends additional credence to the proposed scenario. In this plate there is a fairly extensive enhanced Doppler region centered on beam 13 and some indication of localized enhanced receding velocities on beams 1 and 2. Presumably the former region is related to the irregularity region at the eastern edge of Plate 1*e* and the latter two regions are the remnants of the two original Doppler enhancements. The displacements would indicate that the two original Doppler enhancements were moving

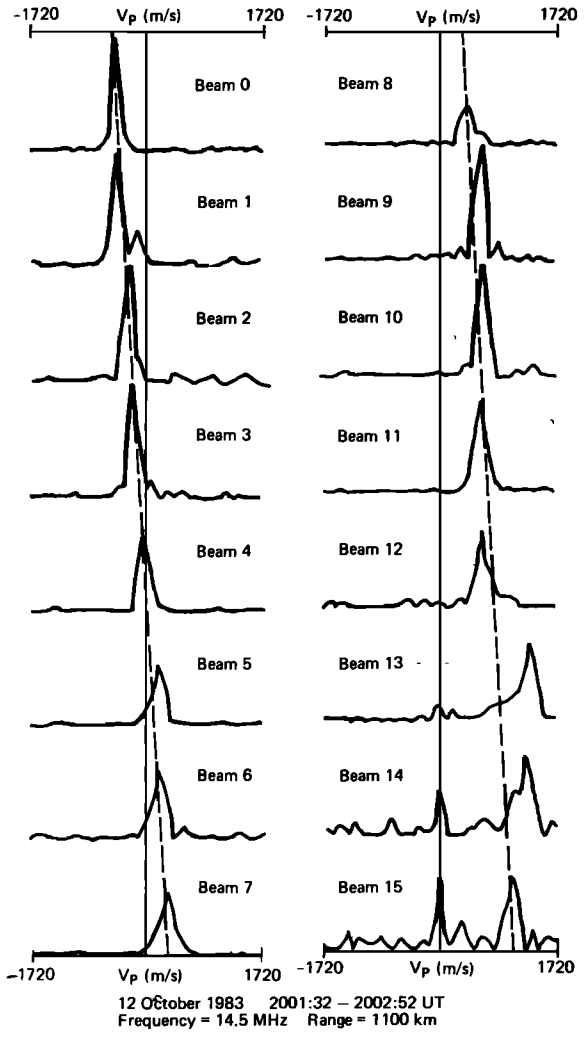

Fig. 12. Azimuthal variation of *F* region irregularity Doppler spectra as observed on October 12, 1983, at 2001:32 UT. The spectra were obtained along an approximately straight line that was directed approximately through the regions of strongest backscattered signal as a function of azimuth in Plate 1*b*. Note that the spectral width is relatively independent of viewing angle.

westward at velocities approximating 1600 m/s, whereas the new region was moving westward at only 800 m/s.

Another approach to studying the drift motion of small-scale ionospheric irregularities is to examine the azimuthal variation of their Doppler spectral characteristics. This approach may also aid in the identification of the mechanisms that produce the irregularities. Figure 12 exhibits the Doppler spectral variation that we have observed in association with Plates 1*b* and 1*e*. The spectra were obtained along an approximately straight line that passes through the regions of strongest backscatter and runs from slightly south of west to slightly north of east. This line skirts along the poleward edge of the two enhanced Doppler regions on beams 6 and 9. It should be noted that the spectra from each beam have different normalizations, and thus there is no significance to the spectral amplitudes.

Several interesting features are to be noted in Figure 12. First, all of the spectra have relatively narrow Doppler widths. Most of these widths range from 200 to 300 m/s, which is not appreciably wider than the Doppler resolution associated with the 17-lag autocorrelation function analysis ($\sim$110 m/s). Second, there is little systematic variation of the Doppler width with viewing direction. In particular, the spectra do not become broad when the radar is directed normal to the irregularity drift direction. This is contrary to the behavior of *E* region irregularity spectra at VHF and UHF frequencies (see, for example, *Greenwald et al.* [1975] and *Tsunoda* [1976]).

Third, aside from those beams on which the selected spectra were associated with enhanced Doppler values (i.e., beams 5, 9 and 10, and 13 and 14), the spectra exhibit a remarkably linear variation of Doppler shift with viewing direction. This is to be expected over the azimuth sector scanned if the measured Doppler velocity is the projection of the mean irregularity convection velocity onto the radar viewing direction. Finally, from the slope of the Doppler variation, as defined by the dashed line, one can estimate the mean convection velocity as slightly south of westward with a speed of $\sim$1750 m/s. This estimate is quite consistent with the velocity estimates that were obtained from the westward movement of the enhanced Doppler regions.

A second example of observations that have been made with the Goose Bay radar is shown in Plates 2*a*–2*f*. These data were obtained on October 16, 1983, between 0204 UT and 0213 UT. This is approximately 2 hours before local midnight. One can see in Plates 2*a*–2*c* that the scattering regions in this case are localized amorphous structures with spatial dimensions of 100–400 km. The structures appear to be moving along a channel that extends from the northeastern to the southwestern edges of the field of view. When the structures are first observed at a range of 2000 km, they are quite faint; however, they intensify as they move equatorward. It is quite possible that this is only an apparent intensification of the structures resulting from their moving to higher elevation angles as they approach the radar. At the

higher elevation angles the antenna array is appreciably more sensitive.

Of the two structures seen in Plate 2*a*, it appears that the poleward structure is moving faster and also in a more southerly direction. This can be seen from the displacement of the structures during the 400 s of observation. (The backscattered signal at the equatorward edge of the field of view in Plate 2*a* appears to be a ground return and will be ignored.) From the displacement of the structures, one can calculate their drift velocities. These calculations indicate that the equatorward structure appears to be moving in a west-southwesterly direction at a speed of 700 m/s, whereas the poleward structure appears to be moving in a south-southwesterly direction at a speed of 1000 m/s.

The Doppler data shown in Plates 2*d*–2*f* are quite consistent with the spatial movement of structures. One sees that the equatorward structure initially exhibited a Doppler speed of 500 m/s and slowed to 200 m/s over the interval of investigation. The poleward structure initially indicated a Doppler velocity of nearly 1000 m/s, and it slowed to 500 m/s. Both of these Doppler observations are consistent with a model in which high-speed irregularity structures slow down and turn westward as they drift out of the polar cap and into the late evening auroral zone.

DISCUSSION

While this paper has been intended primarily to describe the new JHU/APL HF radar located at Goose Bay and to illustrate some of its capabilities, it is already possible to highlight some of the initial results. First, it is clear from our observations, including those presented here, that the small-scale irregularities to which the radar is sensitive are produced over large areas extending for hundreds of kilometers. This observation imparts certain restrictions on the mechanisms that might form small-scale structures. For example, various gradient instabilities require that larger-scale density gradients be present to produce small-scale structure. If small-scale irregularities are observed over an extended volume, then larger-scale gradients must also fill this volume. These larger-scale structures, if present, should be observable with other techniques such as satellite beacon scintillation studies.

Second, it is interesting to note that the spatial anisotropy of the small-scale scattering regions in the afternoon and late evening sectors is similar to the spatial anisotropy of medium-scale irregularity structure as it is observed in these local time sectors. That is, in the afternoon and evening sectors the medium-scale irregularity structures have a much greater east-west than north-south extent, and they are referred to as sheetlike, whereas near midnight, as the medium-scale irregularity structures exit the polar cap they are nearly isotropic and referred to as rodlike [*Livingston et al.*, 1982]. Similar anisotropy characteristics are observed for the spatial extent of the small-scale scattering regions described in this paper.

Third, it is important to note that both the observed spatial displacements of the irregularity structure reported here and the Doppler data obtained from these irregularities are entirely consistent with the expected plasma convection for the local times considered. To some extent, this is to be expected, since both electrons and ions drift together at *F* region heights. Moreover, proposed *F* region instability mechanisms are very low frequency phenomena with near zero phase velocities in the plasma reference frame [e.g., *Reid*, 1968; *Ossakow and Chaturvedi*, 1979; *Hudson and Kelley*, 1976]. Thus the velocity that the ground-based observer will measure is most likely to be that due to the plasma drift. One of our immediate goals is to test this hypothesis more fully by comparison of the Goose Bay radar data with data from the Sondrestrom and Millstone Hill incoherent scatter radars. Concurrent observations have already been made with these facilities, and the results of this study will be reported in the near future.

Finally, our initial spectral observations, including those illustrated in Figure 12, have yielded interesting results. One is struck by the narrowness of the Doppler spectra in all viewing directions and particularly when the radar is directed normal to the irregularity drift direction. Under similar conditions, high-latitude *E* region Doppler spectra would have exhibited widths in excess of 1200 m/s (see, for example, *Greenwald et al.* [1975] and *Ecklund et al.* [1975]). Possibly, this narrowness may be related to the low-frequency nature of the *F* region plasma instabilities that may be exciting small-scale irregularities.

Earlier work by *Hanuise et al.* [1981] exhibited both narrow and broad spectra, while observations reported by *Greenwald et al.* [1983] indicated spectra that were a factor of 2 broader than those reported here. Possibly, some of these differences may be explained by differences in instrumentation. However, it is clear that additional spectral studies are required to confirm the observations reported in this paper.

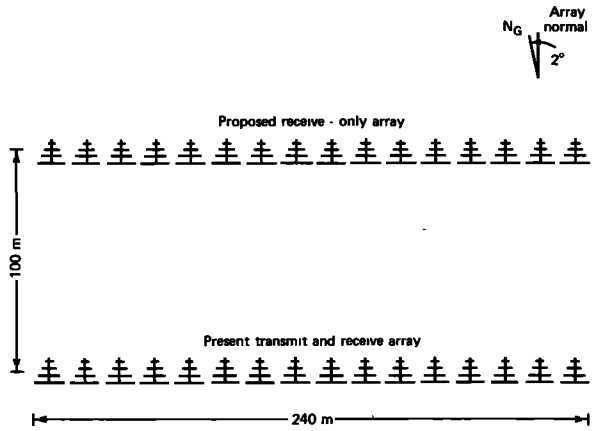

Fig. 13. View of present and planned antenna configurations at the Goose Bay site. The additional 16-element array will enable the vertical angle of arrival of the backscattered signals to be determined to an accuracy of 1°.

FUTURE PLANS

Although the JHU/APL HF radar at Goose Bay is already a sophisticated instrument, it will be upgraded in two significant ways during the current year. As we have noted at the beginning of this paper, a second similar facility is being planned for installation near James Bay, Quebec. This radar is being constructed by a group of French institutions with one of the authors (C. H.) as lead investigator. The radar should begin limited operation in the fall of 1984. Full operation will commence in 1985. With the two radars operating together, it will be possible to obtain two Doppler components from each scattering volume and, thereby, derive two-dimensional drift maps in the manner of the STARE and SABRE radars (see, for example, *Greenwald et al.* [1977]). Because HF radars can sense irregularities in both the *E* and *F* regions of the ionosphere, the common volume of the planned joint measurements will be nearly a factor of 7 greater than that of either STARE or SABRE. Thus very large areas of the high-latitude ionosphere may be imaged. In particular, it will be possible to study the structure and dynamics of irregularity motion in the vicinity of the polar cusp.

Since HF investigations are often prone to directional ambiguity as a result of ionospheric refraction along the ray path, operation of the second radar will have an additional benefit. By combining simultaneous observations from the two radars it should be possible to locate the scattering volume more accurately in both height and direction. It would also be possible to obtain a better understanding of the precise effects that ionospheric refraction have on high-latitude HF propagation. (Although a significant amount of thought has been given to the selection of a name or acronym for the combined radar system, no suitable choice has yet been found. Any suggestions for this name will be gratefully received, and, if selected, the person suggesting the name will not only have the satisfaction of having named the system, but also, this person will receive a good bottle of French wine.)

The second upgrade will be made directly to the Goose Bay radar in the summer of 1984. At that time an additional array of 16 antennas will be added to the existing array, as shown in Figure 13. Each array will be phased independently through the same phasing matrix, however, the new array will only be used for reception. The signals received by the two arrays will be sampled in the present manner and, in addition to calculating the autocorrelation function of the received signal, it will be possible to calculate the cross-correlation function of the combined signals. This technique has been used with considerable success by the Cornell group [*Farley et al.*, 1981]. The Fourier transforms of the autocorrelation and cross-correlation functions will yield the coherency of the Doppler spectrum at each frequency as well as the phase lag between the signals arriving at the two antenna arrays. The latter piece of information may be converted directly to the vertical angle of arrival of the returning signal, which we expect to determine to an accuracy of better than 1°.

Precise knowledge of the vertical angle of arrival will improve greatly our ability to determine the height of the scattering layer as well as the variation of this height with frequency. Information of this type will aid in the identification of the processes leading to the formation of small-scale ionospheric structure at high latitudes, and it will improve our understanding of the effects that high-latitude electron density structure has on HF propagation.

In summary, we expect the existing and planned HF radars described in this paper to provide significant new data that will improve our understanding of (1) high-latitude ionospheric irregularities in both the *E* and *F* regions, (2) high-latitude propagation, and (3) the dynamics of the high-latitude ionosphere.

Note added in proof. The French HF radar is currently being installed at Schefferville, Quebec. This site is located approximately 800 km northeast of the James Bay site shown in Figure 2.

Acknowledgments. The Goose Bay radar was initially funded by the Aeronomy Program Area of the Atmospheric Sciences Division of the National Science Foundation under grant ATM-

8216571. Additional monetary and manpower support were provided by the Atmospheric Sciences Division of the Air Force Office of Scientific Research, the Atmospheric Effects Division of the Defense Nuclear Agency, the Ionospheric Physics Branch of the Air Force Geophysics Laboratory, the Electromagnetic Propagation Branch of Rome Air Development Center, and the Internal Research and Development Program of JHU/APL. Particular thanks are due to those individuals who were in various ways associated with the development of the radar. They include J. Waaramaa, R. Galik, K. Degen, R. Gowell, and J. Winterbottom of the Air Force Geophysics Laboratory; J. Kelsey, W. Conkie, and B. Gill of Canada Marconi; M. Pinnock of the British Antarctic Survey; R. Drake and T. Stevenson of 438 MAW, MAC, USAF; J. Walsh of the Canadian Department of Public Works; and A. W. Bennett, G. Palmer and the members of the JHU/APL Electronics Fabrication Group. One of the coauthors (C. H.) is also supported in part by an NSF-CNRS scientific exchange stipend. A portion of the travel funds was provided by NATO grant 529/83 for colloborative research.

REFERENCES

Baker, K. B., R. A. Greenwald, and R. T. Tsunoda, Very high latitude *F* region irregularities observed by HF radar backscatter, *Geophys. Res. Lett.*, *10*, 904, 1983.

Bates, H. F., and P. R. Albee, Aspect sensitivity of *F* layer HF backscatter echoes, *J. Geophys. Res.*, *75*, 165, 1970.

Ecklund, W. L., B. B. Balsley, and R. A. Greenwald, Crossed-beam measurements of the diffuse radar aurora, *J. Geophys. Res.*, *80*, 1805, 1975.

Farley, D. T., Multiple-pulse incoherent scatter correlation function measurements, *Radio Sci.*, *7*, 661, 1972.

Farley, D. T., H. M. Jerkic, and B. G. Fejer, Radar interferometry: A new technique for studying plasma turbulence in the ionosphere, *J. Geophys. Res.*, *86*, 1467, 1981.

Fremouw, E. J., and J. M. Lansinger, Dominant configurations of scintillation-producing irregularities in the auroral zone, *J. Geophys. Res.*, *86*, 10,087, 1981.

Greenwald, R. A., W. L. Ecklund, and B. B. Balsley, Diffuse radar aurora: Spectral observations of non–two-stream irregularities, *J. Geophys. Res.*, *80*, 131, 1975.

Greenwald, R. A., K. B. Baker, and J. P. Villain, Initial studies of small-scale *F* region irregularities at very high latitudes, *Radio Sci.*, *18*, 1122, 1983.

Hanuise, C., J.-P. Villain, and M. Crochet, Spectral studies of *F* region irregularities in the auroral zone, *Geophys. Res. Lett.*, *8*, 1083, 1981.

Hudson, M. K., snd M. C. Kelley, The temperature gradient drift instability at the equatorward edge of the ionospheric plasma trough, *J. Geophys. Res.*, *81*, 3913, 1976.

Kelley, M. C., J. F. Vickrey, C. W. Carlson, and R. Torbert, On the origin and spatial extent of high-latitude *F* region irregularities, *J. Geophys. Res.*, *87*, 4469, 1982.

Livingston, R. C., C. L. Rino, J. Owen, and R. T. Tsunoda, The anisotropy of high latitude nighttime *F* region irregularities, *J. Geophys. Res.*, *87*, 10,519, 1982.

Ossakow, S. L., and P. K. Chaturvedi, Current convective instability in the diffuse aurora, *Geophys. Res. Lett.*, *6*, 332, 1979.

Reid, G. C., The formation of small-scale irregularities in the ionosphere, *J. Geophys. Res.*, *73*, 1627, 1968.

Tsunoda, R. T., Doppler velocity maps of the diffuse radar aurora, *J. Geophys. Res.*, *81*, 425, 1976.

Vickrey, J. F., C. L. Rino, and T. A. Potemra, Chatanika/TRIAD observations of unstable ionization enhancements in the auroral *F* region, *Geophys. Res. Lett.*, *7*, 789, 1980.

K. B. Baker, R. A. Greenwald, and R. A. Hutchins, Johns Hopkins University Applied Physics Laboratory, Johns Hopkins Road, Laurel, MD 20707.

C. Hanuise, Laboratoire de Sondages Electromagnétiques de l'Environnement Terrestre, Université de Toulon, Boulevard des Armaris, Toulon 83100, France.